A ROBUST BAYESIAN AGENT FOR OPTIMAL COLLISION AVOIDANCE MANOEUVRE PLANNING

C. Greco, L. Sánchez, M. Manzi, and M. Vasile

University of Strathclyde, Glasgow, UK,
Email: {c.greco, luis.sanchez-fdez-mellado, matteo.manzi, massimiliano.vasile}@strath.ac.uk

ABSTRACT

This paper addresses the problem of automatically allocating Collision Avoidance Manoeuvres under uncertainty by a robust Bayesian framework. This framework allows propagating the objects' uncertainty, predicting collisions, allocating manoeuvres, updating the state estimation with Bayesian inference, and redefining the manoeuvres, accounting at all steps for aleatory and epistemic uncertainty. The Bayesian framework combines a robust particle filter for state estimation and uncertainty propagation, an intelligent agent for automatically classifying risk events and allocating avoidance manoeuvres, and a Collision Avoidance Manoeuvre optimiser for obtaining the optimal manoeuvre. A test case is included to show the operation of the system. Two scenarios are presented: a collision and a near-miss conjunction.

Keywords: Robust Bayesian Estimation; Intelligent Agent; Collision Avoidance Optimisation; Epistemic Uncertainty.

1. INTRODUCTION

In a context where the space environment around the Earth is becoming more and more populated, current tools to deal with classical operational problems have to be updated [12].

One key aspect that has to be enhanced is the automation of tasks, both on-board the satellite and in ground facilities. In Space Traffic Management (STM), under a situation of an increasing number of conjunctions alerts, certain processes have to be automated for the sake of sustainability [13]. This is the case of close encounters detection, but also the proper identification of the most appropriate action in the face of a potential collision or the allocation of avoidance manoeuvres.

Artificial Intelligence (AI) can play an important role on this regard. It has the ability of learning from data and creating its own models that can be used as surrogates of more complex dynamical or empirical models. It is also possible to employ them for creating support decision agents able to handle several pieces of information, related in a more or less complex way, at the same time. Along with the capacity to provide faster results once trained, AI appears as a promising tool for automation in space [2, 11].

As important as automation is the way we deal with uncertainty on state estimation and orbit propagation. State estimation techniques on collision avoidance and object tracking usually rely on single well-defined distributions. However, this relies only covariance estimates and covariance realism [14], without no information on the uncertainty distribution and neglecting some sources of uncertainty coming from the lack of knowledge of the system, i.e., non perfectly modelled dynamics, non full characterised sensors... Since the increasingly impact of the decisions affecting one satellite to future potential conjunctions and other object's operation, a more robust approach to deal with aleatory and epistemic uncertainty, as the imprecise probabilities approach [1], has to be contemplated.

On this paper, we propose a Bayesian framework for automatically allocate Collision Avoidance Manoeuvres (CAMs). This system aims to close the loop of state estimation, uncertainty propagation, decision-making on the event of a potential collision and CAM execution. The framework combines a robust approach, accounting for aleatory and epistemic uncertainty at all the steps, with AI to support the operators on the decision making.

The paper is structured as follows. In Section 2, we present the context within the Bayesian framework is developed. The remainder of the paper will detail the different modules that comprise the system. The robust Bayesian estimation will be first introduced in Section 3 before presenting the Intelligent Classification System and the Collision Avoidance Manoeuvre Optimiser in Sections 4 and 5, respectively. In Section 6, we introduce a test case to show the operation of the Bayesian framework. We close the paper in Section 7 with the final remarks.

2. BAYESIAN FRAMEWORK

The Bayesian framework we present in this paper is immersed within the *Computer Agent for Space Situational Awareness aNd Debris Remediation Automation* (CASSANDRA) we are developing at University of Strathclyde. CASSANDRA is an Intelligent Agent for Space Environment Management (SEM) designed to tackle some of the problems the space environment is expected to face in the near future. It is constituted by different modules to address different aspects affecting the safety operation of the satellites: space objects tracking, uncertainty quantification and propagation, anomaly detection, space weather forecasting, or application of AI for STM.

Two main drivers on the development of CASSANDRA are the use of AI and the treatment of uncertainty. AI techniques are employed to extract information from available data in order to make predictions in satellites' state or in space weather, but also for supporting operators with decision-making aid tools or for modelling the long-term evolution of the space environment. Regarding the uncertainty, we aim to widen the perspective on its modelling by incorporating not only aleatory, but also epistemic uncertainty. While the former is inherent to the process and cannot be reduced, the latest refers to the lack of knowledge on the process or the limitations on the modelling of the phenomenon. It could be reduced if more information about the system was available.

In this context, the Bayesian framework we present in this work aims to automatically allocate CAMs for close encounters affected by aleatory and epistemic uncertainty. With this system, we intent to close the loop between sate estimation, uncertainty propagation, risk assessment under potential collisions, decision-making, CAM performance and observations acquisition.

Fig. 1 shows the pipeline of the system. Given an uncertain initial state distribution and the dynamics to propagate the uncertainty, it is possible to estimate the object's state distribution at future times. We are able to include sparse noisy measurements on the process and update sequentially the uncertain state at any time new observations are received through a sequential Bayesian estimator. A robust particle filter allows the computation of the posterior state distributions and the expectation on the probability of impact accounting, at all steps, for aleatory and epistemic uncertainty.

The system is able to provide feedback with the most suitable action to be taken when a close encounter is detected. It will perform a risk assessment using an AI-based classification system that considers the proximity of the encounter as well as the uncertainty affecting the state. On the one hand, for events presenting low-risk, the suggestion will be to take no further actions. On the other hand, on events possessing a higher risk, the need of executing a CAM will be indicated and a the optimal manoeuvre computed by a CAM optimiser. After executing the manoeuvre, the new state can be re-estimated and the risk re-evaluated. Finally, on events affected by a high degree of uncertainty, the output of the system will be to acquire more observations and refine the state estimation before re-assessing the collision risk.

In order to accomplish these tasks, the Bayesian framework presents different modules that relate among each other: a Robust Particle Filter, an Intelligent Classification System and a Collision Avoidance Manoeuvre optimiser. On the following, each of them is introduced in more detail.

3. ROBUST BAYESIAN ESTIMATION

This section describes the *Observations* and *State Estimation* modules in Fig. 1. The probabilistic formulation of the robust estimation problem and the Robust Particle Filter (RPF) approach to compute bounds on a quantity of interest under epistemic uncertainty are presented in this section. Reference [8] describes into greater detail this formulation as well as the filtering approach, whereas here we present a short description of both.

3.1. Estimation model under epistemic uncertainty

The aim is to estimate the state of a continuous-time dynamical system governed by a nonlinear Ordinary Differential Equation (ODE)

$$\dot{\mathbf{x}} = f(t, \mathbf{x}, \mathbf{d}), \tag{1}$$

where $\mathbf{x} \in \mathbb{R}^n$ is the system state and $\mathbf{d} \in \mathbb{R}^d$ are model parameters. Uncertainty affects the knowledge of this dynamical state on both its initial conditions $\mathbf{x}_0 = \mathbf{x}(t_0)$ and static model parameters. Therefore, the system state is not known exactly.

To improve the knowledge of the system state at a later time, indirect noisy measurements of the state are taken at discrete times t_k

$$\mathbf{y}_k = h(t_k, \mathbf{x}_k, \boldsymbol{\varepsilon}_k), \tag{2}$$

for $k = 1, \ldots, M$, with $t_k < t_{k+1}$, and where $\boldsymbol{\varepsilon}_k$ is the observation noise.

The uncertainties in the initial condition, dynamical parameter, and sensor noise are modelled as Random Variables (*RV*s) $\mathbf{X}_0$, $\mathbf{D}$, and $\mathbf{Y}_k$ respectively. Hence, the lower-case quantities $\mathbf{x}_0 \in \boldsymbol{\Omega}_{x_0}$, $\mathbf{d} \in \boldsymbol{\Omega}_d$, and $\mathbf{y}_k \in \boldsymbol{\Omega}_{y_k}$ are specific realisations of these *RV*s within their sample spaces $\boldsymbol{\Omega}_{(\cdot)}$. Let $p(\mathbf{x}_0)$ and $p(\mathbf{d})$ represent the probability density function (pdf) of the corresponding random variables. On the other hand, the uncertainty on the observation is induced by the sensor noise. Thus, the observation uncertainty is modeled by means of the likelihood function $p(\mathbf{y}_k|\mathbf{x}_k)$ as a function of $\mathbf{x}_k$, which describes, given the sensor noise, how likely it is the sample $\mathbf{x}_k$ given the

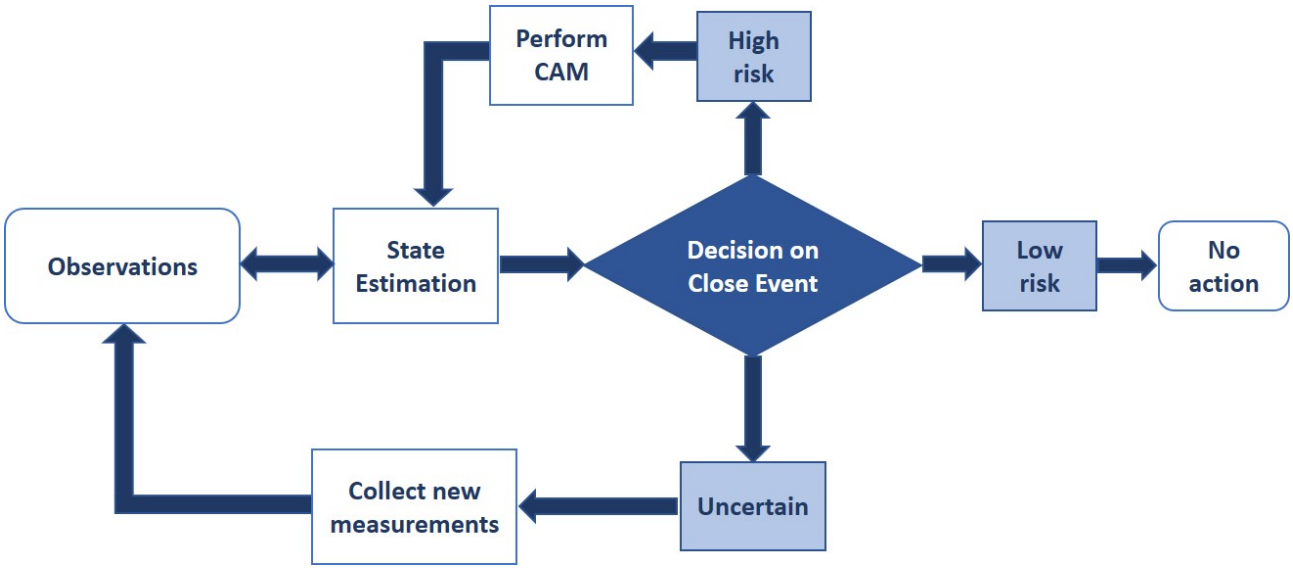

Figure 1: Diagram of robust Bayesian pipeline for optimal collision avoidance manoeuvre planning.

observation $\mathbf{y}_k$ was received. Also, the transition distribution $p(\mathbf{x}_k|\mathbf{x}_{k-1})$ is employed to model the uncertain state propagation in time in a probabilistic fashion.

Given these uncertainty sources, the system state at time t_k, $k > 0$, is uncertain and therefore modelled as a *RV*. Its pdf is a conditional distribution which takes into account the measurements acquired

$$p(\mathbf{x}_k|\mathbf{y}_{1:k}) \,, \tag{3}$$

where $\mathbf{y}_{1:k}$ is the collection of observations up to time t_k. In this model, the posterior distribution (3) is approximated as described in Section 3.2.

In practical applications, the goal is often to optimally estimate a statistical measure of a nonlinear quantity of interest $\phi : \mathbb{R}^n \to \mathbb{R}$ conditional on the received observation. In this paper, the statistical measure employed is the expected value of ϕ with respect to the posterior

$$\mathbb{E}\left[\phi(\mathbf{x}_k)\right] = \int_{\mathbf{\Omega}_{x_k}} \phi(\mathbf{x}_k)\, p(\mathbf{x}_k|\mathbf{y}_{1:k})\, d\mathbf{x}_k \,. \tag{4}$$

The most used measure in satellite collision estimation is the probability of impact between two objects. In this setting, the posterior represents the distribution of the satellites' state modelled as *RV*s, whereas the function ϕ is an indicator function. Let $C \subset \mathbb{R}^n$ be the subset for which a collision happen. Let I_C be the indicator function on the set C

$$I_C = \begin{cases} 1 & \text{if } \mathbf{x}_k \in C \\ 0 & \text{if } \mathbf{x}_k \in C \,. \end{cases} \tag{5}$$

Then, the Probability of Collision (PoC) is defined as the expectation of the indicator function I_C, which is computed by plugging $\phi = I_C(\mathbf{x}_k)$ in Eq. (4) as

$$\text{PoC} = \int_{\mathbf{\Omega}_{x_k}} I_C(\mathbf{x}_k)\, p(\mathbf{x}_k|\mathbf{y}_{1:k})\, d\mathbf{x}_k \,. \tag{6}$$

When epistemic uncertainty is considered, the pdfs are not known precisely but specificed within an imprecise set $\mathcal{P}$. Epistemic models enable more accurate representations of unknown situations in which information is insufficient to characterise specific pdfs.

Here, the set $\mathcal{P}$ is assumed parameterised by an epistemic parameter $\boldsymbol{\lambda} \in \Omega_\lambda$. Hence, for the initial condition, the epistemic set is defined as

$$\mathcal{P}_{x_0} = \left\{ p(\mathbf{x}_0; \boldsymbol{\lambda}_0) \,|\, \boldsymbol{\lambda}_0 \in \Omega_{\lambda_0} \right\}, \tag{7}$$

which degenerates to a singleton in case $\boldsymbol{\lambda}_0$ is precisely known, that is purely aleatory uncertainty. An equivalent definition holds for the other probability functions.

Hence, the epistemic estimation model is formulated as

$$\mathbf{X}_0 \sim p(\mathbf{x}_0; \boldsymbol{\lambda}_0) \qquad \in \mathcal{P}_{x_0} \tag{8a}$$
$$\mathbf{X}_k \sim p(\mathbf{x}_k \,|\, \mathbf{x}_{k-1}; \boldsymbol{\lambda}_{x_k}) \in \mathcal{P}_{x_k|x_{k-1}} \tag{8b}$$
$$\mathbf{Y}_k \sim p(\mathbf{y}_k \,|\, \mathbf{x}_k; \boldsymbol{\lambda}_y) \qquad \in \mathcal{P}_{y_k|x_k}. \tag{8c}$$

This epistemic model induces a set of posterior distributions parameterised in $\boldsymbol{\lambda}_k = [\boldsymbol{\lambda}_0, \boldsymbol{\lambda}_{x_k}, \boldsymbol{\lambda}_y]$

$$p(\mathbf{x}_k \,|\, \mathbf{y}_{1:k}; \boldsymbol{\lambda}_k) \in \mathcal{P}_{x_k} \,. \tag{9}$$

Consequently, the expectation of interest (4) depends on the epistemic parameter $\boldsymbol{\lambda}_k$ as well

$$\mathbb{E}\left[\phi(\mathbf{x}_k); \boldsymbol{\lambda}_k\right] \,. \tag{10}$$

Therefore, the sought result of the epistemic estimation is an interval, whose bounds are the lower and upper values of the expectation of interest. By definition, the lower and upper bounds are the minimum and maximum of the expectation as

$$\underline{\mathbb{E}}\left[\phi(\mathbf{x}_k)\right] = \min_{\boldsymbol{\lambda}_k \in \Omega_{\boldsymbol{\lambda}_k}} \mathbb{E}\left[\phi(\mathbf{x}_k); \boldsymbol{\lambda}_k\right] \tag{11a}$$
$$\overline{\mathbb{E}}\left[\phi(\mathbf{x}_k)\right] = \max_{\boldsymbol{\lambda}_k \in \Omega_{\boldsymbol{\lambda}_k}} \mathbb{E}\left[\phi(\mathbf{x}_k); \boldsymbol{\lambda}_k\right] . \tag{11b}$$

3.2. Robust Particle Filter

The Bayesian RPF approach to compute such bounds is shortly described in the this section.

In the sequential Bayesian framework adopted, the generic posterior is computed by iterating two fundamental steps:

- *uncertainty propagation*: the posterior distribution at time t_{k-1} is propagated to time t_k through the ODEs

$$p(\mathbf{x}_{k-1}|\mathbf{y}_{1:k-1}) \rightarrow p(\mathbf{x}_k|\mathbf{y}_{1:k-1})\,. \tag{12}$$

  The resulting distribution is called prior at time t_k.

- *observation update*: at a discrete instance, the prior distribution is updated to incorporate the last observation according to the unnormalised sequential Bayes' rule

$$p(\mathbf{x}_k|\mathbf{y}_{1:k}) \propto p(\mathbf{y}_k|\mathbf{x}_k)\,p(\mathbf{x}_k|\mathbf{y}_{1:k-1})\,. \tag{13}$$

By iterating these steps from t_0 to t_k, the posterior distribution can be obtained.

The steps highlighted above do not have an analytical computation procedure for generic uncertainty distributions, nonlinear dynamical and observation models. Thus, the posterior distribution (3) is a non-parametric complex pdf. Hence, the integral (4) does not have a closed-form solution. Furthermore, it is often impractical to draw samples from a non-parametric distribution, making also its numerical approximation challenging.

By using importance sampling and the sequential nature of the estimation problem (8), an estimator of the expectation is constructed as

$$\mathbb{E}\left[\phi(\mathbf{x}_k);\boldsymbol{\lambda}_k\right] \approx \hat{\theta}\big(\boldsymbol{\chi}_{0:k};\boldsymbol{\lambda}_k\big) = \textstyle\sum_{i=1}^{N} \hat{w}_k^{(i)}(\boldsymbol{\lambda}_k)\,\phi(\mathbf{x}_k^{(i)}), \tag{14}$$

that is a weighted sum of ϕ evaluations on fixed samples and importance weights which depend on the epistemic parameters. The symbol $\boldsymbol{\chi}_{0:k} = \{\mathbf{x}_{0:k}^{(1)}, \ldots, \mathbf{x}_{0:k}^{(N)}\}$ indicates the collection of N trajectories represented by samples at $k+1$ discretised times. The samples $\mathbf{x}_k^{(i)}$ are drawn from a proposal distribution $\pi(\mathbf{x}_k \,|\, \mathbf{x}_{0:k-1}, \mathbf{y}_{1:k})$ which does not depend on the epistemic parameter. The importance weights are computed sequentially as

$$w_k^{(i)}(\boldsymbol{\lambda}) = \frac{p(\mathbf{y}_k \,|\, \mathbf{x}_k^{(i)};\boldsymbol{\lambda}_y)\; p(\mathbf{x}_k^{(i)} \,|\, \mathbf{x}_{k-1}^{(i)};\boldsymbol{\lambda}_x)}{\pi(\mathbf{x}_k^{(i)} \,|\, \mathbf{x}_{0:k-1}^{(i)}, \mathbf{y}_{1:k})}\; \hat{w}_{k-1}^{(i)}(\boldsymbol{\lambda}) \tag{15a}$$

$$\hat{w}_k^{(i)}(\boldsymbol{\lambda}) = \frac{w_k^{(i)}(\boldsymbol{\lambda})}{\sum_{j=1}^{N} w_k^{(j)}(\boldsymbol{\lambda})}, \tag{15b}$$

from $\hat{w}_0^{(i)}(\boldsymbol{\lambda}_0) = p(\mathbf{x}_0^{(i)};\boldsymbol{\lambda}_0)/\pi(\mathbf{x}_0^{(i)})/N$. Because Eq. (13) is the unnormalised Bayes' update, Eq. (15b) self-normalises the weights to ensure the estimator coherence.

In this way, the weights, which are dependent on the epistemic parameter, and the particle sampling, which is independent of the epistemic parameter, are decoupled. As a result, once the particles have been drawn from the proposal and propagated in time, the optimisation problems (11) can be performed simply by working on the weights. Indeed, the particles sampling, pdf and function evaluations, can all be precomputed before the optimisation cycles.

A bound estimator is constructed by minimising/maximising the estimator $\hat{\theta}\big(\boldsymbol{\chi}_{0:k};\boldsymbol{\lambda}_k\big)$ over $\boldsymbol{\lambda}_k$

$$\underline{\hat{\theta}}\big(\boldsymbol{\chi}_{0:k}\big) = \min_{\boldsymbol{\lambda}_k \in \Omega_{\boldsymbol{\lambda}_k}} \hat{\theta}\big(\boldsymbol{\chi}_{0:k};\boldsymbol{\lambda}_k\big) \tag{16a}$$

$$\overline{\hat{\theta}}\big(\boldsymbol{\chi}_{0:k}\big) = \max_{\boldsymbol{\lambda}_k \in \Omega_{\boldsymbol{\lambda}_k}} \hat{\theta}\big(\boldsymbol{\chi}_{0:k};\boldsymbol{\lambda}_k\big). \tag{16b}$$

These optimisation problems are generally nonlinear and multimodal. Therefore, a Branch & Bound (B&B) approach over simplicial subdomains exploiting the estimator Lipschitz continuity is developed in [8]. This algorithm ensures asymptotic convergence to the global bound and a measure of the distance from it at each iteration.

4. INTELLIGENT CLASSIFICATION SYSTEM

This section describes the *Decision on Close Event* module of Fig. 1. In particular, we present a Machine Learning (ML) based Intelligent Classification System (ICS) to automatically allocate the most appropriate action to be taken by an operator under the event of a close encounter. This ICS was first introduced in [15]. It provides the optimal action to be considered by an operator, encoded as a 5-class category, according to the risk and uncertainty of the event. This recommendation ranges from designing or executing a CAM (classes 1 and 2) or to collecting more measurements (class 3) or not taking further actions (classes 5 and 4).

The system is able to handle both epistemic and aleatory uncertainty. The later is modelled with a multidimensional Normal distribution of the relative position on the impact plane (defined by the mean and covariance matrix), while the epistemic uncertainty is quantified with the lower and upper expectation of the relative position.

4.1. Classification criterion

Here, we present the epistemic classification criterion in which the ICS is based on to classify the events. This criterion classifies a close encounter event based on: the time to the Time of Closest Approach (TCA) and two

epistemic variables: the lower expectation and the degree of confidence (the difference between the upper and lower expectation) of the probability of collision, P_C, being bigger than a certain threshold, P_{C0}. Oppositely to the common probabilistic approaches, where the decision is made exclusively based on the value of the computed PoC to raised binary alert flags (i.e. collision/no-collision), this method works with the confidence on the correctness of the value of PoC in order to provide a more complete information. Thus, the outcome of the classification criterion is not only able to indicate if an event is high risk or low risk, but also if it is affected by a high degree of uncertainty.

The expectation on the value of the PoC being bigger than a certain threshold should be understand as the support from the available information than the PoC, is at least, as high as that value. In case the lower expectation at the specified P_{C0} is great enough, it should be understood as there is enough support from all the information obtained that the value of the P_C is at least as high as the threshold. In case the difference between lower and upper expectation (degree of confidence) is greater than a specific value at the threshold, it means the event is affected by a high degree of uncertainty: some piece of the available information indicates the PoC could be higher than the threshold, while another piece of information is not confident with that proposition. The operator cannot be confidence either in defining the event as high-risk or low-risk encounter.

It is worth mentioning that the lower and upper expectation on the PoC being bigger than the threshold is computed from the bounded expectation of the relative position components at the impact plane and the elements of the associated covariance matrix that can be obtained after propagating the uncertain estimated state to the encounter.

The output of the criterion is a 5-class classification aiming to properly address the uncertainty associated to the events and, therefore, provide a more meaningful decision to the operators. This five classes can be grouped on: high risk events, classes 1 and 2, which require a CAM (*High risk* modules on Fig. 1); low risk events, classes 4 and 5, where no further action is needed (*Low risk* and *No action* modules on Fig. 1); event highly affected by uncertainty, class 3, where more observations should be acquired before making any decision on the manoeuvring (*Uncertain* and *Collect new measurements* modules on Fig. 1).

Table 1 summarises the criterion. Three different aspects are considered: i) the time to the encounter from the last observation, dividing the events in short-term, mid-term and long-term according to two time thresholds, T_1 and T_2; ii) the value of PoC above of which there is no support for higher values, measured with a threshold on the lower expectation, $\underline{\mathbb{E}}_0$; iii) and the degree of confidence at a certain value of probability of collision, P_{C0} indicating the degree of uncertainty affecting the event and evaluating according to a threshold value, Δ. More details on the epistemic classification criterion can be found in [15].

Table 1: Epistemic classification criterion.

Time to TCA	PoC for $\underline{\mathbb{E}} = \underline{\mathbb{E}}_0$	Degree of confidence at P_{C_0}	Class
$t_{TCA} < T_1$	$P_{C_e} \geq P_{C_0}$	-	1
	$P_{C_e} < P_{C_0}$	$\overline{\mathbb{E}} - \underline{\mathbb{E}} \leq \Delta$	5
		$\overline{\mathbb{E}} - \underline{\mathbb{E}} > \Delta$	1
$T_1 \leq t_{TCA}$ $t_{TCA} < T_2$	$P_{C_e} \geq P_{C_0}$	-	2
	$P_{C_e} < P_{C_0}$	$\overline{\mathbb{E}} - \underline{\mathbb{E}} \leq \Delta$	5
		$\overline{\mathbb{E}} - \underline{\mathbb{E}} > \Delta$	3
$T_2 \leq t_{TCA}$	$P_{C_e} \geq P_{C_0}$	-	2
	$P_{C_e} < P_{C_0}$	$\overline{\mathbb{E}} - \underline{\mathbb{E}} \leq \Delta$	4
		$\overline{\mathbb{E}} - \underline{\mathbb{E}} > \Delta$	3

4.2. Machine Learning based classification system

Based on the previous epistemic classification criterion a ML-based ICS is used for automatically classify uncertain close encounters.

The ML technique we used in this work for the ICS is Random Forests (RF). On previous works by the authors [15] different techniques (Random Forests, Artificial Neural Networks, Support Vector Machine and K-Nearest Neighbours) were used for predicted the class, showing that RF performed the best.

Given an uncertain close encounter, the outcome of the ICS is the risk class indicating the most suitable action according to the epistemic criterion based on the proximity of the encounter and the uncertainty associated with the event. On the aforementioned work, the authors tested the ICS following two different strategies, differing in the type of inputs provided to the system: on the first one, the inputs were the same parameters used on the epistemic criterion (time to TCA, and the Lower expectation and the Degree of Confidence of the PoC being bigger than a threshold); on the second strategy, the inputs where the time to the TCA and the lower and upper expectation of the variables defining the relative geometry: the two components of the relative position on the impact plane and the three elements of the covariance matrix modelling the aleatory uncertainty on the position. In this work, the second strategy has been followed since the accuracy achieved is comparable on both strategies. The selected strategy presents, also, the advantage of bypassing the explicit computation of the lower and upper expectations of $P_C \geq P_{C0}$, but instead using the bounded expectation of the encounter geometry variables (miss distance and rela-

tive position covariance matrix elements) provided by the propagation in Section 3.

The outcome of the ICS can be then used on the context of the Bayesian framework. According to the provided output, more measurements may be obtained or the state re-estimated after a CAM execution, before re-assessing the risk with the ICS.

5. COLLISION AVOIDANCE MANOEUVRE OPTIMISATION

This section illustrates the *Perform CAM* module of Fig. 1. Specifically, it introduces the Collision Avoidance Manoeuvre model to compute the optimal CAM in those cases that require a correction in the orbits for avoiding a potential collision. This allows us to close the loop between state estimation, decision-making and CAM performance.

5.1. Collision Avoidance Manoeuvre formulation

The optimal CAM is generated by solving the following bilevel optimisation problem

$$\begin{aligned} &\min_{\Delta\mathbf{v}} \ \|\Delta\mathbf{v}\| \\ &\text{s.t. } \overline{\text{PoC}} < \varepsilon \,, \end{aligned} \tag{17}$$

where

$$\overline{\text{PoC}} = \max_{\boldsymbol{\lambda}\in\Omega_\lambda} \text{PoC} \,. \tag{18}$$

Therefore, the optimal impulsive manoeuvre minimises the propellant expenditure while realising a PoC below the safe threshold ε even in the epistemic worst case scenario. The safe PoC threshold is set to $\varepsilon = 10^{-6}$ according to European Space Agency's (ESA) guidelines [4].

Specifically, in this work the PoC in Eq. (6) is computed by means of the indicator function of a condition on the Distance of Closest Approach (DCA) between the two space objects. By having the state vector composed by the states of the two objects under consideration $\mathbf{x} = \left[\mathbf{x}^{(1)}, \mathbf{x}^{(2)}\right]$, the collision indicator is

$$I_C = \begin{cases} 1 & \text{if } DCA(\mathbf{x}^{(1)}, \mathbf{x}^{(2)}) \leq \delta_C \\ 0 & \text{if } DCA(\mathbf{x}^{(1)}, \mathbf{x}^{(2)}) > \delta_C \,. \end{cases} \tag{19}$$

where δ_C is a collision threshold depending on the satellites' geometrical characteristics. The DCA for two objects in a close encounter is computed as the pericentre distance of their relative hyperbolic trajectory [19].

5.2. Execution error

When computing the PoC, it is important to account for possible deviations due to execution errors on the CAM. Indeed, the executed CAM will differ from the commanded one due to pointing errors, thrust inaccuracies, time delays and so on.

In this work, the adopted model for execution errors on the CAM manoeuvre follows the Gates' model [5, 6] (see Figure 2). This model was already employed in the context of robust manoeuvre optimisation under uncertainty in [7]. Here we report a short description of this model.

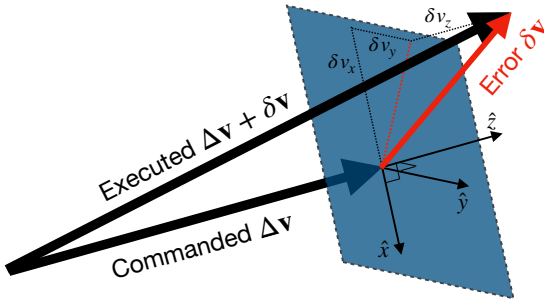

Figure 2: Model for execution error.

The error $\delta\mathbf{v}$ is decomposed in modulus and angular variations on the nominal manoeuvre $\Delta\mathbf{v}$. In a frame centred in the spacecraft with the z-axis aligned with $\Delta\mathbf{v}$, the y-axis perpendicular to both the $\Delta\mathbf{v}$ and the ecliptic normal, and the x-axis completing the right-handed frame, the execution error components are taken from zero-mean normal distributions

$$\begin{aligned} \delta v_x &\sim \mathcal{N}(0, \sigma_{pf}^2 + \sigma_{pp}^2 \|\Delta\mathbf{v}\|) \\ \delta v_y &\sim \mathcal{N}(0, \sigma_{pf}^2 + \sigma_{pp}^2 \|\Delta\mathbf{v}\|) \\ \delta v_z &\sim \mathcal{N}(0, \sigma_{mf}^2 + \sigma_{mp}^2 \|\Delta\mathbf{v}\|) \,. \end{aligned} \tag{20}$$

The parameters σ_{mf} and σ_{mp} indicate the standard deviations of the fixed and proportional magnitude components respectively, whereas σ_{pf} and σ_{pp} define the corresponding pointing components. The error in the local frame is then rotated into the inertial one where $\Delta\mathbf{v}$ is defined to achieve the error $\delta\mathbf{v}$ The executed control is the sum of the nominal manoeuvre and the error.

Eq. (20) defines the aleatory uncertainty on the CAM manoeuvre. If the parameters for the Gates' model are only partially known, e.g. due to poorly characterisation of the thrusting engine or a low Technology Readiness Level (TRL) engine, epistemic uncertainty should be modelled by defining the parameters as interval-valued [7].

6. CASE STUDY

This section discusses the operational scenarios on which the robust Bayesian agent is tested.

6.1. Satellite conjunction setup

The conjunction under consideration is between the operation satellite SENTINEL 2B (NORAD ID 42063) and a piece of debris from FENGYUN 1C (NORAD ID 30141). On the 7th of January 2021, SOCRATES (Satellite Orbital Conjunction Reports Assessing Threatening Encounters in Space) [18] reported a potential collision between these objects at reference Time of Closest Approach (rTCA) 13-Jan-2021 at 13:24:25 UTC. The orbital elements for SENTINEL 2B and FENGYUN 1C DEB are reported in Table 2.

Table 2: Objects orbital elements from NORAD TLEs.

NORAD ID	42063	30141
EPOCH [UTC]	08/01/21 01:17:15	07/01/21 16:24:07
a [km]	7167.14	7180.78
e [-]	1.1e-4	2.5e-3
i [deg]	98.57	99.08
Ω [deg]	85.33	183.01
ω [deg]	81.09	252.25
M [deg]	279.04	107.59

The dynamical system is described in Cartesian coordinates within an Earth-centered inertial reference frame. The dynamical forces included are: Earth gravity with harmonics up to degree and order 4; atmospheric drag using Jacchia-Gill model; soli-lunar third-body gravitational attraction; the solar radiation pressure with a conical shadow model for Earth's eclipses.

At first, we assume the operational satellite is perfectly tracked, e.g. due to GPS receivers, and therefore the uncertain state to estimate is the one of the piece of debris, that is $\mathbf{x} = \mathbf{x}^{(2)}$.

Observations are simulated to improve the knowledge of the debris state. The measured quantities are the debris azimuth and elevation with respect to the equatorial plane [17] obtained by means of optical measurements.

6.2. Uncertainty models

Normal distributions are considered to model the pdf of the initial condition

$$\mathbf{X}_0 \sim \mathcal{N}\left(\mathbf{x}_0; \boldsymbol{\mu}_0, \boldsymbol{\Sigma}_0\right) . \tag{21}$$

The mean $\boldsymbol{\mu}_0$ is set to the Cartesian state resulting from the orbital elements in Table 2. The covariance $\boldsymbol{\Sigma}_0$ is constructed by taking typical errors associated to Two-Line Elements (TLE) from ESA guidelines [9]. The 1σ uncertainty on TLE for objects characterised by inclinations larger than 60 deg is summarised in Table 3 in radial, transversal and normal components. The covariance

Table 3: 1σ position (r) and velocity (v) uncertainty of TLEs for orbits with $e < 0.1$, $i > 60$ deg, perigee altitude $\leq 800km$, in radial (U), transversal (V), and normal components (W).

Component	Value	
$1\sigma_{r_U}$	104	[m]
$1\sigma_{r_V}$	556	[m]
$1\sigma_{r_W}$	139	[m]
$1\sigma_{v_U}$	559	[mm/s]
$1\sigma_{v_V}$	110	[mm/s]
$1\sigma_{v_W}$	148	[mm/s]

$\overline{\boldsymbol{\Sigma}}_0$ resulting from these standard deviations is then rotated in the standard Cartesian inertial frame by using the Jacobian of the radial-transversal-normal transformation.

However, the uncertainties in Table 3 are just presumed [9] and therefore far from being well-characterised. Furthermore, because different sets of TLEs are usually estimated from different measurements stations, it may be impossible to define a single covariance which properly characterises the TLE uncertainty. Hence, epistemic uncertainty is introduced on the covariance by parameterising $\boldsymbol{\Sigma}_0$ using two epistemic parameters $\boldsymbol{\lambda}_0 = [\lambda_{0-1}, \lambda_{0-2}]$. The covariance parameterisation reads as follows

$$\boldsymbol{\Sigma}_0(\boldsymbol{\lambda}_0) = \begin{bmatrix} \lambda_{0-1}\overline{\boldsymbol{\Sigma}}_0(1:3,1:3) & \mathbf{0}_{3\times3} \\ \mathbf{0}_{3\times3} & \lambda_{0-2}\overline{\boldsymbol{\Sigma}}_0(4:6,4:6) \end{bmatrix} , \tag{22}$$

that is the epistemic parameters scale respectively the position and velocity blocks of the reference covariance $\overline{\boldsymbol{\Sigma}}_0$ computed as above. The bounds considered for these multipliers are $\lambda_{0-1}, \lambda_{0-2} \in [1/5^2, 5^2]$, that is they can change the reference 1σ uncertainties by roughly shrinking them up to $1/5$, or expand them by a factor of 5. The measurements are simulated using the debris reference trajectory and then adding the sensor errors, drawn from a zero-mean normal distribution with diagonal covariance $\boldsymbol{\Sigma}_y$. The reference uncertainty on the measurement is set to $1\sigma_{y_{az}} = 1\sigma_{y_{el}} = 10$ arcsec. Given that the optical measurements are acquired from non-professional stations, these 1σ values were again obtained from the literature and are not coming from a rigorous sensor characterisation. Thus, epistemic uncertainty is considered on the noise covariance by means of two parameters $\boldsymbol{\lambda}_y = [\lambda_{y-az}, \lambda_{y-el}]$. The epistemic parameters range is set to $\lambda_{y-az}, \lambda_{y-el} \in [1/5^2, 5^2]$, in line with diverse 1σ values found in literature [16, 3, 10].

The parameters for the Gates' execution error (see Section 5.2) are set in Table 4.

6.3. Classification thresholds

The values of the thresholds used by the ICS for risk assessment (see Section 4.1) are shown on Table 5.

Table 4: Gates' parameters for execution errors.

Component	Value	
σ_{pf}	3.0	[mm/s]
σ_{pp}	7.0	[mrad]
σ_{mf}	5.0	[mm/s]
σ_{mp}	.33%	[-]

They include the two time thresholds (T_1, T_2) to discern among short-term, mid-term and long term encounter; the threshold on probability of collision (P_{C_0}) at which evaluate the lower expectation and the Degree of Confidence; the value of the lower expectation at which the trust on the value is lost $(\underline{\mathbb{E}}_0)$; and the value of the Degree of Confidence above which the event is considered to be highly affected by uncertainty (Δ).

Table 5: ICS thresholds values.

Threshold	Value	
T_1	2.0	[days]
T_2	4.0	[days]
P_{C_0}	10^{-6}	[-]
$\underline{\mathbb{E}}_0$	0.5	[-]
Δ	0.3	[-]

6.4. Results

Two operational scenarios are considered, one resulting in a collision and one near-miss conjunction.

Collision scenario

In this case, the true unknown trajectory of the FENGYUN 1C DEB debris eventually results in a collision with SENTINEL 2B. We assume observations are available up to 48 hours before rTCA.

The result of the robust Bayesian estimation at this point is displayed in Fig. 3. In the plot, several 3σ ellipses, which correspond to different values of the epistemic parameters, are displayed. The collision probability is robustly estimated as

$$\text{PoC} \in [0, 2 \cdot 10^{-4}].$$

Hence, the ICS is hence run to analyse the conjunction. The classification returns a class 3 scenario, that is a highly uncertain conjunction which requires further measurements to take an informed action. Therefore, the agent decides to wait for new measurements until the next checkpoint, 24 hours before rTCA.

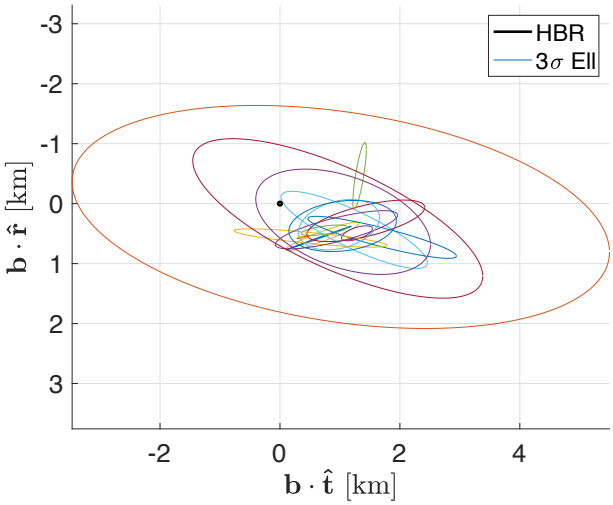

Figure 3: B-plane 3σ ellipses for collision scenario with observations up to 48h before TCA.

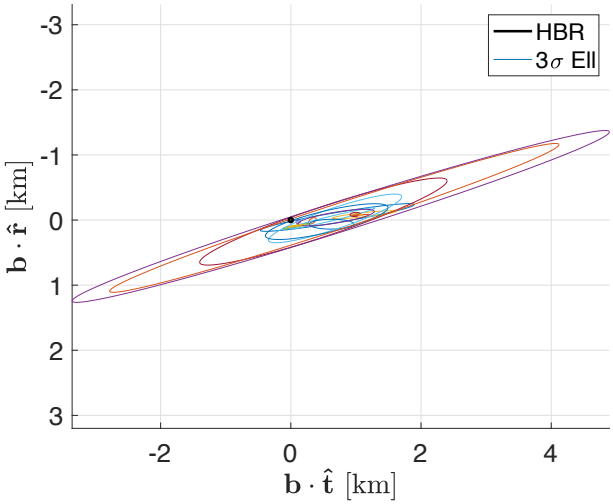

Figure 4: B-plane 3σ ellipses for collision scenario with observations up to 24h before TCA.

At this point, after new observations are available, the robust Bayesian estimation is rerun and the results displayed in Fig. 4. The collision probability is now

$$\text{PoC} \in [0, 1.8 \cdot 10^{-3}].$$

The ICS return a class 1 conjunction, that is a high risk event which require a CAM.

Thus, the CAM module is run to design a robust and optimal manoeuvre which realise a $\overline{\text{PoC}}$ smaller than 10^{-6} while taking into account state and CAM execution errors. The CAM on SENTINEL 2B is designed 10 revolutions before the rTCA.

After the manoeuvre execution, the robust estimation is run again to check that the upper collision probability indeed satisfies the safety threshold in the presence of state and execution errors. The resulting graph is shown

in Fig. 5, where it can be seen that there is no intersection between the 3σ ellipses and the Hard-Body Radius (HBR).

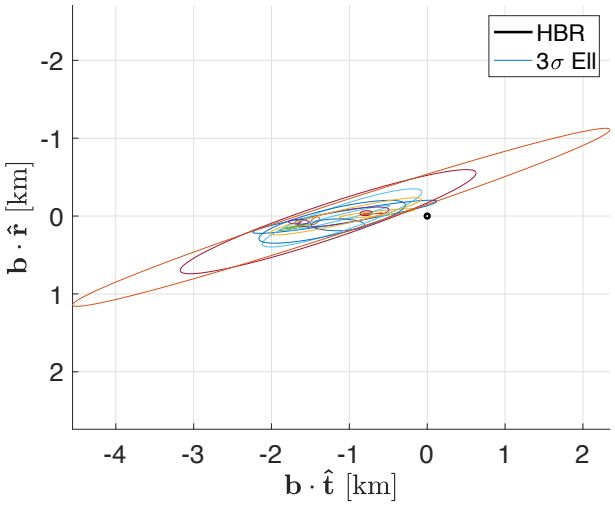

Figure 5: B-plane 3σ ellipses for collision scenario after CAM.

The upper probability bound post CAM is $\overline{\text{PoC}} < 10^{-7}$.

The evolution of the PoC bounds at the several checkpoints considered is shown in Figure 6.

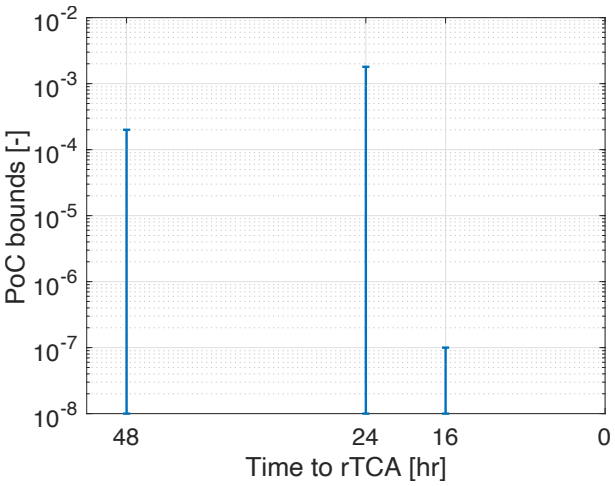

Figure 6: Evolution of PoC bounds for collision scenario.

No-collision scenario

In this scenario, the true unknown trajectory of the FENGYUN 1C DEB debris misses SENTINEL 2B by ≈ 2 km. Again, we start assuming observations are available up to 48 hours before rTCA.

The result of the robust Bayesian estimation 48 hours before rTCA is depicted in Fig. 7. The robust probability

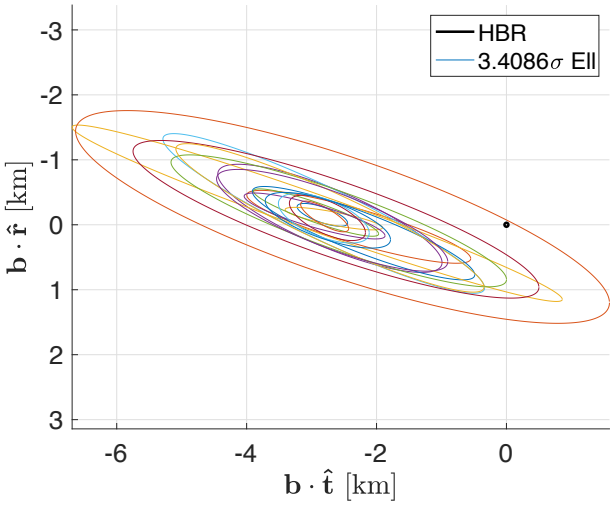

Figure 7: B-plane 3σ ellipses for no-collision scenario with observations up to 48h before TCA.

interval is

$$\text{PoC} \in [0, 1.8 \cdot 10^{-4}].$$

Thus, the conjunction analysis is similar to the collision one at 48 hours before rTCA. The ICS is run and it return a class 3 conjunction, again labelling a highly uncertain scenarios and the need for further measurements to implement an informed action.

Further measurements are acquired until the 24 hours checkpoint, where the Bayesian estimation is updated. The resulting conjunction geometry is displayed in Fig. 8. Here, it can be seen how the debris 3σ ellipses are rather

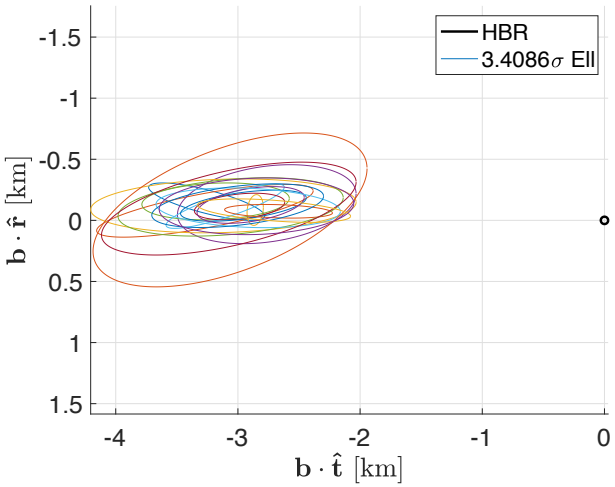

Figure 8: B-plane 3σ ellipses for no-collision scenario with observations up to 24h before TCA.

distant from the HBR of the operational satellite, and indeed centred on the true (unknown) trajectory. The ICS returns a class 5 conjunction labelling a safe conjunction. Indeed, the corresponding upper probability is estimated to be $\overline{\text{PoC}} < 10^{-10}$. The intelligent agent therefore requires no further action.

For the no-collision scenario, the PoC bounds estimated at the two different checkpoints are displayed in Figure 9.

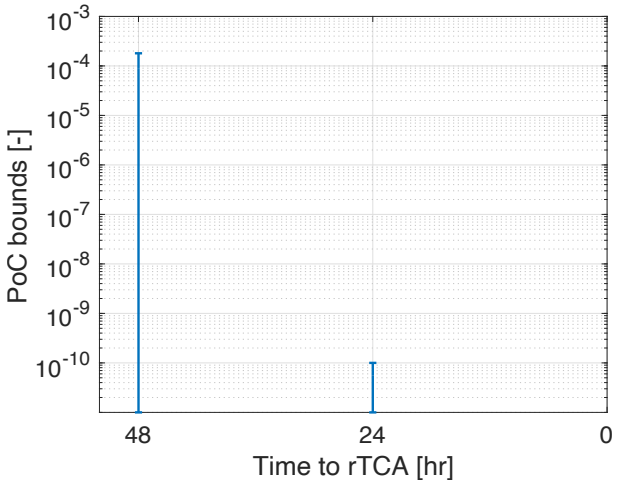

Figure 9: Evolution of PoC bounds for no-collision scenario.

7. CONCLUSION

This paper proposes a robust Bayesian framework for automatic Collision Avoidance Manoeuvre allocation. This framework combine Artificial Intelligence and a Robust Particle Filter able to handle aleatory and epistemic uncertainty to close the loop between sequential state estimation, uncertainty propagation, close encounter risk evaluation and decision-making, and CAM execution. The term robust refers to the definition of manoeuvres that are guaranteed to avoid a collision under aleatory and epistemic uncertainty in the prediction of the probability of collision.

The Bayesian framework is an essential module on the structure of CASSANDRA. CASSANDRA is and intelligent agent we are developing at University of Strathclyde for addressing problems related with Space Environment Management. Within this framework, we present a system able to automatically allocate CAM through an intelligent system able to propose the most suitable action for a close encounter based on the available information. This intelligent system received information about the expected values of the encounter geometry from a robust Bayesian estimator and, at the same time, provides feedback to the estimator to update the state based on new acquired measurements or the new state after a CAM execution.

This framework is constituted by three main modules that relate among each other. The first of them is a robust Bayesian particle filter for state estimation and orbit propagation. This system is able to sequentially update the state estimation when receiving/simulating new measurements through and efficient robust particle filter. It accounts for aleatory and epistemic uncertainty on the initial state distribution and the noise affecting the measurements. It can provide the lower and upper expectations of any encounter related metric, as it can be the impact plane relative position parameters. The second module is an intelligent classification system that makes use of Random Forest algorithms to automatically indicate the most convenient action to be taken when a close encounter is detected. By receiving the bounded expectation provided by the previous module, it gives a 5-class classification indicating if an event is high-risk, low-risk or highly uncertain, being needed to perform a CAM, not take further actions, or gather more observations, respectively. The third module computes the optimal CAM on those high-risk events to steer the thrusting spacecraft on a safe trajectory. Aleatory and epistemic uncertainties are considered on the state knowledge and manoeuvre errors, which are included to model inevitable errors in the CAM execution. The manoeuvre is designed such that the post-CAM upper collision probability is below a safety threshold set to 10^{-6}.

The operation of the system has been shown with a test case between the operational satellite SENTINEL 2B and a piece of space debris from the FENGYUN 1C. The initial state and the measurements have been considered to be affected by uncertainty. The aleatory uncertainty has been modelled by normal distributions. The epistemic uncertainty has been modelled through interval-valued parameters scaling the covariance matrices. Two scenarios have been tested: one leading to a collision, the other to a close encounter, but not a collision. In both cases, the initial uncertain state has been propagated and updated with measurement using the robust Bayesian estimator and the Robust Particle Filter before preforming a risk assessment. Then, the Intelligent Classification System has been used for indicating the most suitable actions. Through both scenarios, the three possibilities have been shown: obtaining more measurement to reduce the uncertainty of the event, executing a CAM for avoiding a potential collision, and taking no further actions in case of a safe encounter. In all cases, after executing the appropriate action, the state has been re-estimated to re-evaluate the encounter risk. On the collision scenario, it is shown the CAM optimiser provides an optimal and robust manoeuvre accounting for the uncertainty affecting the state and including the uncertainty introduced by the manoeuvre itself.

ACKNOWLEDGMENTS

This work was funded by the European Commission's H2020 programme, through the H2020-MSCA-ITN-2016 UTOPIAE Marie Curie Innovative Training Network, grant agreement no. 722734; by the European Comission's H2020 program, through the H2020-MSCA-ITN-2018 STARDUST-R Marie Curie Innovative Training Network, grant agreement no. 813644; and by the European Space Agency, through the Idea I-2019-01650.

REFERENCES

1. Augustin T., Coolen F. P. A., De Cooman G., Troffaes M. (2014). Introduction to Imprecise Probabilities, *John Wiley & Sons*
2. Benjamin Bastida V., Flohrer T., Krag H., Merz K., Lemmens S. (2019). CREAM - ESA's proposal for collision risk estimation and automated mitigation, *1st International Orbital Debris Conference*, Sugar Land, Texas, USA.
3. Bennett, J. C., Sang, J., Smith, C., Zhang, K. (2015). An analysis of very short-arc orbit determination for low-Earth objects using sparse optical and laser tracking data, *Advances in Space Research*, Elsevier, vol. 55 (2), pp 617–629.
4. Braun V., Flohrer T., Krag H., Merz K., Lemmens S., Virgili B. B., Funke Q. (2016). Operational support to collision avoidance activities by ESA's space debris office, *CEAS Space Journal*, Springer, vol. 8 (3), pp 177–189.
5. Gates, C. R. (1963), A simplified model of midcourse maneuver execution errors, *Jet Propulsion Laboratory, California Institute of Technology*.
6. Goodson, T. D. (2013). Execution-error modeling and analysis of the GRAIL spacecraft pair, *23rd AAS/AIAA Spaceflight Mechanics Meeting*.
7. Greco, C., Campagnola, S., Vasile, M. (2020). Robust space trajectory design using belief stochastic optimal control, *AIAA Scitech 2020 Forum*.
8. Greco C., Vasile M. (under review). Robust Bayesian Particle Filter for Space Object Tracking Under Severe Uncertainty, *Journal of Guidance, Control, and Dynamics*.
9. Klinkrad, H., Alarcon, J. R., Sanchez, N. (2005). Collision avoidance for operational ESA satellites, *4th European Conference on Space Debris*, vol. 587.
10. Li, B., Sang, J., Zhang, Z. (2016). A real-time orbit determination method for smooth transition from optical tracking to laser ranging of debris, *Sensors*, Multidisciplinary Digital Publishing Institute, vol. 16 (7).
11. Mashiku A., Frueh C., Memarsadeghi N., Gizzi N., Zielinki M., Burton A. (2019). Predicting satellite close approaches in the context of artificial intelligence, *AAS/AIAA Astrodynamics Specialist Conference*, Portland, Maine, United States.
12. Muelhaupt T., Sorge M., Morin J., Wilson R. (2019). Space traffic management in the new space era, *Journal of Space Safety Engineering*, Elsevier, vol. 6 (2), pp 80–87
13. Nag S., Murakami D., Lifson M., Kopardekar P. (2018). System autonomy for space traffic management, *2018 IEEE/AIAA 37th Digital Avionics Systems Conference (DASC)* .
14. Poore A. B., Aristoff J. M., Horwood J. T., Armellin R., Cerven W. T., Cheng Y., Cox C. M., Erwin R. S., Frisbee J. H., Hejduk M. D., et al. (2016). Covariance and uncertainty realism in space surveillance and tracking, *Tech. rep., Numerica Corporation Fort Collins United States*.
15. Sánchez L., Vasile M., (2020). On the Use of Machine Learning and Evidence Theory to Improve Collision Risk Managment, *Acta Astronautica. ICSSA-2020 Special Issue*, Elsevier
16. Sang, J., Smith, C. (2011). An analysis of observations from EOS space debris tracking system, *11th Australian Space Science Conference*, pp 179–189.
17. Schutz, B., Tapley, B., Born, G. H. (2004). Statistical orbit determination, *Elsevier*.
18. SOCRATES - Satellite Orbital Conjunction Reports Assessing Threatening Encounters in Space. (2019). `http://celestrak.com/SOCRATES/`
19. Wakker, K. F. (2015). Fundamentals of astrodynamics, *TU Delft Library*.